Journal of The
Electrochemical Society

Mitigation of Pitting on Nitrogen-Doped Niobium Surfaces through Two-Step Electropolishing

To cite this article: V. Chouhan *et al* 2025 *J. Electrochem. Soc.* **172** 023502

Journal of The Electrochemical Society, 2025 **172** 023502

Mitigation of Pitting on Nitrogen-Doped Niobium Surfaces through Two-Step Electropolishing

V. Chouhan,[1,z] T. Ring,[1] G. Wu,[1] and E. Viklund[1,2]

[1]*Fermi National Accelerator Laboratory, Batavia, Illinois 60510-0500, United States of America*
[2]*Department of Materials Science and Engineering, Northwestern University, Evanston, Illinois 60208, United States of America*

Surface processing of niobium superconducting RF cavities used in particle accelerators is crucial for determining their performance. The nitrogen (N)-doping method, developed at Fermilab, enhances the cavities' quality factor by doping the cavity's interior surface with N atoms at 800 °C. After N-doping, electropolishing (EP) is employed to remove the niobium nitride phases and attain the desired concentration of interstitial N atoms. This study explores the effects of EP conditions on N-doped niobium samples. The samples were electropolished at 5 to 40 °C and voltages between 3 and 22 V. Different EP voltage ranges produced two types of pits, classified based on their sizes. Larger pits, linked to higher voltages, are also affected by the reaction rate. Pitting could be reduced at a lower temperature and adequate EP voltage. However, to effectively minimize gas evolution forming large-sized pitting, peeling off the top nitride layer before EP might be beneficial. This was achieved through precise low-voltage etching, forming a two-step EP process. The process involves removing the top 100–200 nm layer at a low voltage, followed by standard EP to remove the required material. This two-step EP process effectively mitigated the pitting risk associated with gas evolution on N-doped surfaces.

 [DOI: 10.1149/1945-7111/adaef4]

Manuscript submitted September 17, 2024; revised manuscript received January 21, 2025. Published February 5, 2025.

Superconducting radio frequency (SRF) cavities made of niobium (Nb) are utilized in modern superconducting accelerators, operating in a superconducting state sustained at 2 K through liquid helium. The efficacy of these cavities significantly impacts the operational costs of these machines. The cavities with high accelerating gradients and quality factors (Q_0) are processed with electropolishing (EP) to produce the desired interior surfaces of the cavities.[1] A smooth surface without damage or defect is crucial to attain good SRF performance.[2–8] The etched grain boundaries and defects, including sharp edges, protrusions, and pits, are potential causes of surface magnetic field enhancement that breaks the superconductivity locally, leading to quenching at a lower accelerating field.[2–5] Magnetic field enhancement studies have been conducted systematically on the artificially created pits[4] and the natural pit found on the cavity surface[5] to understand and develop a relation between a pit shape and magnetic field enhancement factor (β_M). As studied by Kubo,[5] a pit geometry characterized by the ratio of the edge radius (r_e) to the radius of the pit (R) and the slope angle ($\pi\alpha$) of the pit wall significantly affects β_M value. A lower surface resistance corresponding to a higher Q_0 value of the SRF cavities is also desired to alleviate cryogenic operational loads at 2 K. Fermi National Accelerator Laboratory introduced a surface processing technique known as nitrogen doping (N-doping), which diffuses nitrogen atoms into the RF penetration layer of the cavities.[9,10] In this process, the cavity is treated in an ultra-high vacuum furnace at 800 °C and under a nitrogen pressure of 25 mTorr to dope the cavity surface with nitrogen atoms. This process substantially boosts the Q_0 of the cavities by at least twofold,[9] as evidenced by R&D cavities,[11] the success of N-doped cavities for the LCLS-II and LCLS-II HE cryomodules,[12] and the marked improvement in 650 MHz Nb cavities.[13]

The N-doping process leads to forming different Nb-N phases, including Nb_2N, which manifest as star- or pyramid-shaped precipitates.[14] Nb_2N is a non-superconducting phase of niobium nitride at the cavity's operating temperature of 2 K.[14–16] The surface with the presence of non-superconducting nitride impurities inadvertently decreases the accelerating field due to premature quenching of the cavity. To address this, the N-doped surface undergoes post-N-doping EP treatment, removing the top layer containing niobium nitride phases while providing the Nb surface with N interstitials.[10] The interstitial N atoms reduce the mean free path to lower *BCS* resistance,[10] ultimately enhancing the Q_0 of the cavity. The thickness of material removed during post-N-doping EP significantly influences cavity performance: a thinner removal decreases the quench field, but excessive removal diminishes the benefits of N-doping's high Q_0.[9] An optimal removal thickness of 5–10 μm maintains a desirable N interstitial concentration, ensuring high Q_0 at a medium field range of 16–25 MV m^{-1} for 1.3 GHz Nb cavities. 1.3 GHz niobium 9-cell cavities, followed by nitrogen doping with optimal EP, for LCLS-II and LCLS-II HE projects consistently met the required performance in terms of accelerating gradient and Q_0.

Standard EP of the Nb cavities is performed with an electrolyte, a mixture of sulfuric (H_2SO_4) and hydrofluoric (HF) acids in a volumetric ratio of 9:1 or 10:1.[17–19] During EP, the cavity temperature is maintained at 20 °C–25 °C. The electrolyte and EP conditions are appropriate for EP of the Nb material. The effect of low temperature, typically ∼15 °C, during EP on the surface morphology was evident as in Refs. 20, 21, where a lower cavity temperature improves the surface smoothness of the Nb cavities. The same electrolyte and conditions are also used for EP the N-doped surface, which might react differently with the electrolyte under the set EP conditions. Cavity temperature during the post-N-doping EP process notably impacts the quench field. A lower surface temperature of 12 °C–15 °C during EP was effective in enhancing the quench field of N-doped cavities.[22] Some studies conducted with samples highlight the effect of EP on N-doped surfaces.[23] The sample EP studies showed pitting and grooves at grain boundaries on the N-doped surface.[23,24] The study in Ref. 23 presented that the pits and grain boundary grooves on the N-doped surfaces might result in magnetic field enhancement and superheating field suppression that could limit the accelerating gradient of N-doped Nb cavities.

Previous studies suggested that the chemistry of the N-doped surface must be conducted safely with adequate parameters to achieve a smooth surface for the N-doped cavities. However, the intricate effects of EP on the N-doped Nb surface remain poorly understood. The EP conditions, which include EP voltage, surface temperature, and HF concentration, still need to be considered in a systematic study to evaluate their impacts on the N-doped surfaces. This paper presents detailed research delving into EP of N-doped Nb samples, elucidating the phenomena observed on the N-doped surface during EP under varied conditions. It proposes a modified EP process to improve surface quality and mitigate pit formation on the surface.

[z]E-mail: vchouhan@fnal.gov

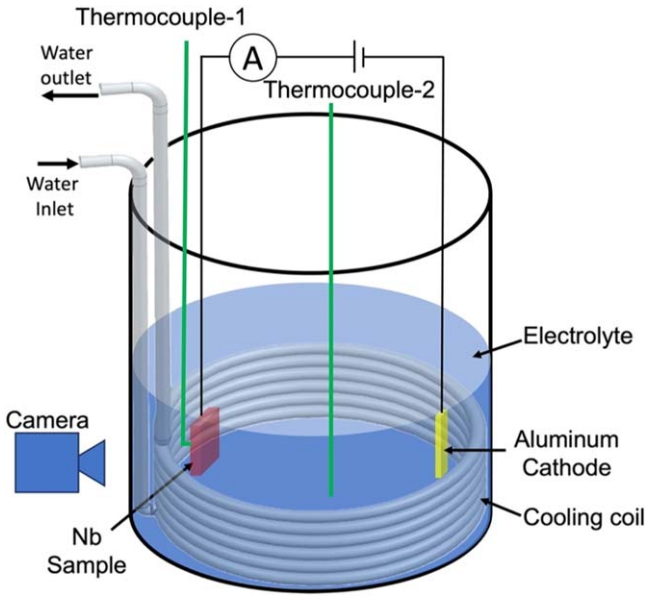

Figure 1. Schematic displaying the setup used for EP Nb samples.

Experimental

EP setup.—EP of Nb samples was conducted in an acid bath employing a two-electrode system, designating Nb and aluminum as the anode and cathode electrodes, respectively (Fig. 1). The Nb samples used in this study were prepared in a size of 10×10 and 20×20 mm from the same Nb sheet with high RRR (residual resistivity ratio) of 300. The cathode surface area was set to be 10% of the Nb surface area. The anode-cathode distance was kept consistent to be ∼10 cm. The EP electrolyte comprised a mixture of H_2SO_4 acid (96 wt%) and HF acid (70 wt%) in a volumetric ratio of 10:1,[19] procured in pre-mixed conditions. In this study, the electrolytes from two different batches procured separately were used. The second batch of the electrolyte possibly had a relatively higher HF concentration. This was observed as a higher value in the EP current density. Each Nb sample was electropolished with a fresh electrolyte having a maximum Nb concentration of $\sim 0.3\ g\ l^{-1}$. To regulate electrolyte temperature, a cooling coil, an aluminum tube coil connected to a chiller flowing temperature-controlled water, was immersed in the electrolyte bath. Thermocouples were fixed on the side wall of the sample and positioned within the electrolyte to monitor real-time sample and electrolyte temperatures during the EP process. A LabVIEW-controlled power supply facilitated adjustable voltage, recording polarization curves (current density J vs voltage V) under varied conditions. EP parameters such as applied voltage, current, sample temperature, and acid temperature were logged at a data sampling time of 250 ms. The EP process was conducted without any agitation to prevent any impact on the surface from acid flow. The acid bath had a transparent wall, allowing visual and optical monitoring. A camera was placed outside the bath to image the EP surface.

Experimental process.—Figure 2 shows a block diagram of the processes applied to these samples. Initially, Nb samples underwent EP for bulk removal of 100 μm, followed by high-temperature furnace treatments involving degassing and N-doping at 800 °C. Bulk EP was conducted at 18 V while maintaining sample temperatures between 25 °C–30 °C. All the samples were ultrasonically cleaned in ultrapure water before the furnace treatment. For N-doping, the standard 2/0 N-doping recipe developed at Fermilab for cavity surface processing was employed, using the same UHV furnace utilized for 800 °C heat treatment and N-doping of Nb SRF cavities. The N-doping process involved raising the furnace temperature to 800 °C at a rate of $3\ °C\ min^{-1}$, holding it at 800 °C for 3 h, introducing N_2 gas at a pressure of 25 mTorr for 2 min, and subsequently ceasing the furnace heaters and gas flow. The temperature and pressure profiles during N-doping are depicted in Fig. 3.

These prepared samples were then subjected to varying conditions of final light EP to examine their impact on surface morphology. The final light EP was executed for a 5–7 μm removal thickness at different sample temperatures and voltages. Furthermore, N-doped samples were immersed in the EP electrolyte for 2–4 h without applied voltage to discern the acid's effect on material etching and surface morphology. The removal thickness in EP was estimated using the weight loss of the samples and Faraday's law of electrolysis.

Surface study.—The sample surfaces underwent examination using a scanning electron microscope (SEM) and laser confocal scanning microscopy (LCSM). LCSM, offering a 3D image and surface profile, provided detailed insights into surface morphology. The images were captured at various sizes of 709×531 μm, 287×215 μm, and 57×43 μm, each with a pixel resolution of 1024×768. The lateral optical resolution for the two smaller fields of view (287×215 μm and 57×43 μm) can reach approximately 0.3 μm. The chemical state of the sample surfaces after N-doping, EP, and exposure to EP-acid were analyzed using energy-dispersive X-ray spectroscopy (EDS) and X-ray photoelectron spectroscopy (XPS). Additionally, byproducts generated during the EP process, to be discussed later, were studied using SEM, EDS, and XPS. The analyzer's pass energy for XPS was set to be 20 eV for narrow scans. The analysis area was set large ($700 \times 250\ \mu m^2$) enough to obtain average information on the chemical state on the surface.

Results

Surface of N-doped sample.—The surfaces of electropolished samples before and after N-doping were observed through SEM to attain typical surface information. Figure 4 displays SEM images of the sample surfaces. The images revealed that the bulk EP surface was smooth with no special surface features. The SEM images of the N-doped surface contained pyramid-shaped features indicative of the nitride phase of Nb. Chemical analysis details are provided in the subsequent section.

Impact of EP-acid exposure.—To assess the influence of the EP acid on the N-doped surface, an N-doped sample was immersed in the EP electrolyte for 2 h at an acid temperature of approximately 23 °C. The sample temperature was continuously monitored from the moment it encountered the acid. The sample temperature remained unaltered during the immersion period. No external cooling was used during this period.

The SEM images of the acid-exposed sample are presented in Figs. 5a–5b. Observable changes in the surface features were noted in SEM. This signified a chemical reaction between the N-doped surface and the EP acid. The distinctive pyramid-shaped features

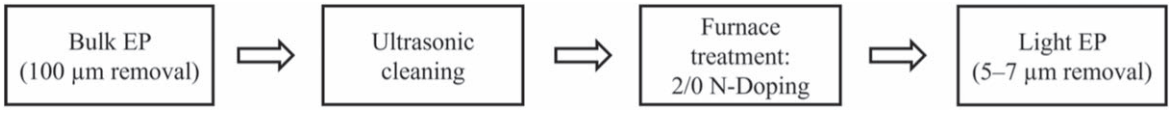

Figure 2. Block diagram illustrating the procedural steps applied to prepare the initial surfaces of Nb samples before their use in the final light EP study to understand the effect of post-N-doping EP on the surface.

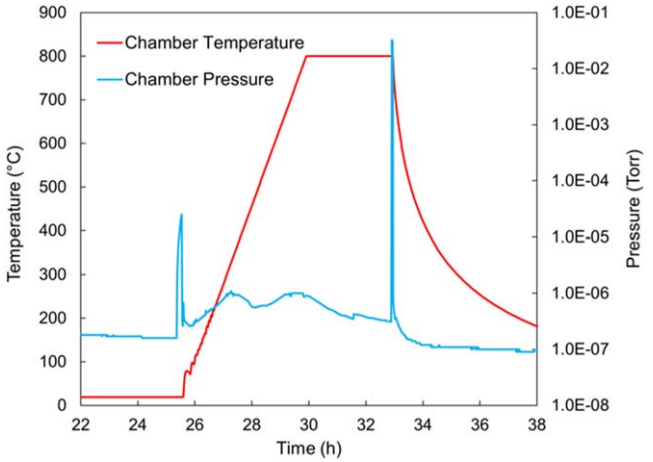

Figure 3. Chamber pressure and temperature profiles recorded during N-doping of the samples in the furnace.

characteristic of the N-doped surface persisted even after the extended acid exposure. The corresponding LCSM 3D image is illustrated in Fig. 5c. The LCSM image revealed that the prolonged acid exposure led to no observable preferential grain etching or pitting on the N-doped.

Electropolishing study.—A detailed EP study was conducted under various conditions to understand their effects on N-doped surfaces.

Polarization curves.—Anodic polarization curves (current density J vs voltage V) provide valuable insights into the chemistry occurring on the anode surface.[25,26] For Nb material, a J–V curve typically displays distinct characteristics across specific voltage ranges: linear, oscillation, and current plateau regions. The linear region, also known as the etching region, produces a rough surface, while the plateau region, referred to as the polishing region, yields a smooth surface. To investigate the differences in surface chemistry between N-doped and undoped samples, J–V curves were measured for both samples under identical conditions. Temperatures for both samples varied from 25 to 48 °C during a voltage rise from 0 to 20 V. The resulting J–V curves are shown in figure 6. Both curves exhibit a similar onset voltage (V_o) of ∼7 V, at which the current starts to plateau, indicating diffusion-limited conditions.[25,27] At higher voltages, starting at 13 V, periodic current oscillations were observed, a regime under which Nb cavities are typically electropolished.[19] The identical J–V curves for both N-doped and undoped samples suggest no significant difference in the EP chemistry between the surfaces.

Effect of temperature.—To examine the effect of EP temperature on N-doped sample surfaces, four N-doped samples, namely ND-18V-5C, ND-18V-15C, ND-18V-24C, and ND-18V-40C, were subjected to light EP at a constant voltage of 18 V and various temperatures ranging from a very low value of 5 °C to a sufficiently high value of 40 °C. Table I shows EP conditions applied to these samples. The sample temperatures during EP were carefully maintained using the cooling coil with a variation of less than ±1 °C. The chiller set temperature was adjusted to maintain the desired sample temperature.

Figure 7 displays sample current density and temperature profiles obtained under the conditions outlined in Table I. Higher temperatures corresponded to higher current densities. The N-doped samples showed typical current density and temperature profiles. Upon voltage application, sample current density and temperature increased, peaking within the first few minutes before stabilizing at lower values. Between the broad peak and initial spike, the current density profiles showed dips. The estimated removal rates were 0.08, 0.16, 0.33, and 0.65 μm min^{-1} at sample temperatures of 5, 15, 24, and 40 °C, respectively.

The N-doped surfaces of these samples were examined using the LCSM, and the corresponding images with different magnifications are shown in Fig. 8. The surface of ND-18V-5C appeared smooth with no observable pits. The surface of ND-18V-15C was also found smooth, except for small shallow pits with a depth of less than 200 nm, which was lower than the macroscopic surface roughness. These pits were present at random locations on the surface and had diameters exceeding 5 μm. These pits were visibly evident on the surfaces of ND-18V-24C and ND-18V-40C, electropolished at 24 °C and 40 °C, respectively. At these higher temperatures, surfaces of

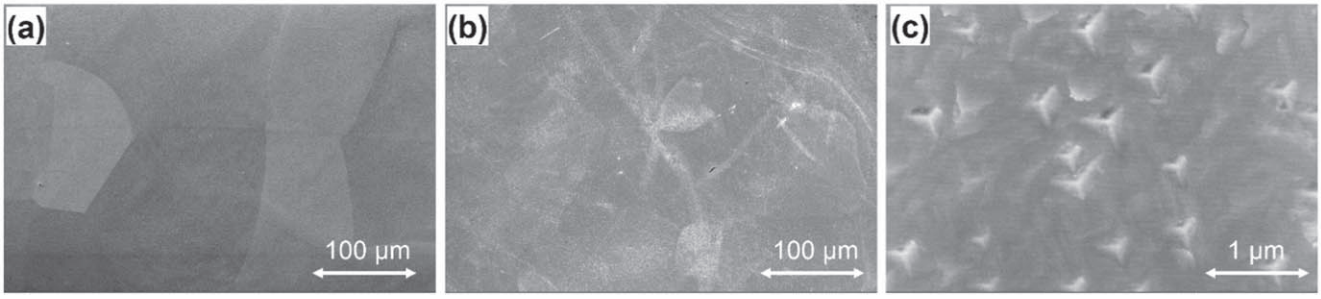

Figure 4. SEM images of the sample surfaces after bulk removal of 100 μm (a) and 2/0 N-doping at 800 °C (b) with magnified surface (c).

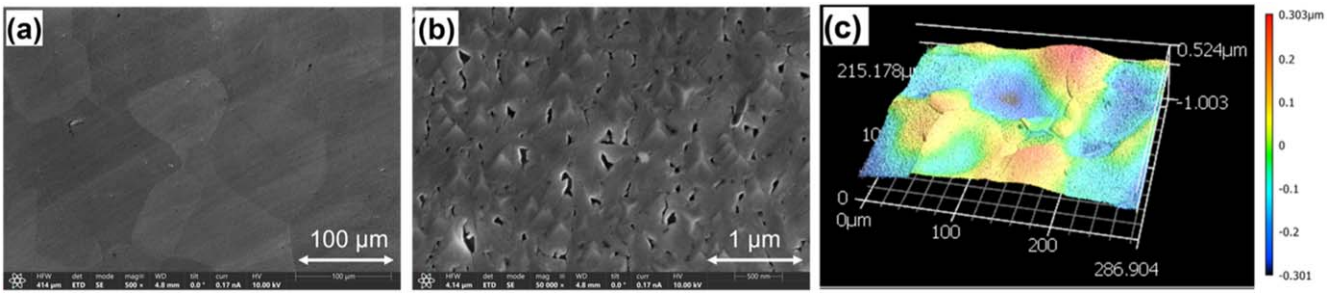

Figure 5. SEM images captured at various magnifications depicting the N-doped surface following a 2 h exposure in EP acid (a) and (b). LCSM image showing the 3D topography of the acid-exposed surface (c).

Table I. Final EP conditions applied to the undoped and N-doped Nb samples. Pre-process represents the process applied before final light EP.

		Light EP	
Sample	pre-process	Sample temperature (°C)	Voltage (V)
ND-18V-5C	Bulk EP, 2/0 N-doping	5	18
ND-18V-15C	Bulk EP, 2/0 N-doping	16	18
ND-18V-24C	Bulk EP, 2/0 N-doping	24	18
ND-18V-40C	Bulk EP, 2/0 N-doping	40	18

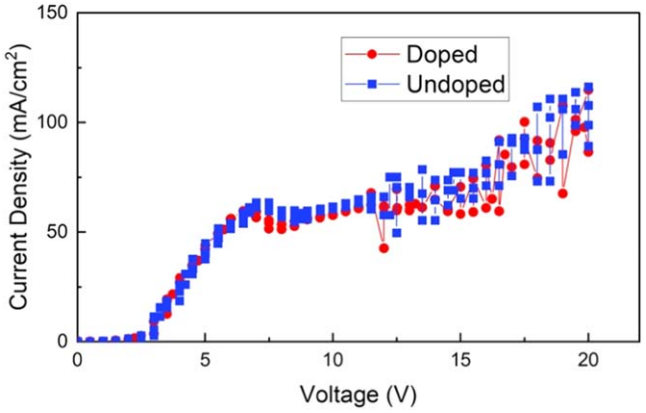

Figure 6. *J–V* curves measured for N-doped and undoped Nb samples in a temperature range of 25 to 48 °C.

ND-18V-24C and ND-18V-40C displayed a higher density of pits, with increasing size and depth as the temperature rose. For ND-18V-24C, pit diameters reached up to 100 μm, with depths of approximately 2 μm. ND-18V-40C displayed even greater pit density with a diameter higher than 100 μm and a depth reaching ∼6 μm.

In this study, the pits were classified into two categories. The pits, present at random locations on the surface and had diameters larger than 5 μm, were called type-1 pits, whereas the pits with comparatively smaller diameters were named type-2 pits. The magnified images, covering a surface area of 57×43 μm^2, were captured to identify small-sized type-2 pits and evaluate microscopic surfaces. The imaging locations were selected to minimize the presence of large-sized type-1 pits observed in the images covering the area of 709×531 μm^2. Although the surfaces were microscopically smooth with no apparent type-2 pits, some grains were found with topographic unevenness. The unevenness here represents surface variation in tens of nanometers. This was noticed in all the N-doped surfaces with different degrees of unevenness. The magnified images of the samples, labeled as zoom-in view, are shown in Fig. 8. The images represent the surface spots with pronounced uneven topographies. As shown in the image, the sample ND-18V-40C treated at 40 °C showed a greater uneven surface than other samples. However, the unevenness on ND-18V-40C remained within 100 nm surface variation.

The typical profiles measured for the type-1 pits observed on ND-18V-15C, ND-18V-24C, and ND-18V-40C are also shown in Fig. 8. The pit geometry parameters, defined in Ref. 5 as r_e/R and $\theta = \pi\alpha$, were evaluated for several deeper type-1 pits found on the surfaces. In most cases, the edge radius r_e exceeded the pit radius R, resulting in $r_e/R > 1$. However, the edges of some pits were non-uniform, leading to lower r_e/R values. For example, a pit on ND-18V-22C was estimated to have $r_e/R = 0.6$ ($R = 33$ μm) and pit-wall angle $\theta = 12°$. Similarly, a pit with radius R of 60 μm on ND-18V-40C was found with $r_e/R = 0.24$ and $\theta = 23°$. No noticeable pits were observed on the undoped surface electropolished at 18 V and given the temperature range. Furthermore, no significant preferential grain etching was observed in either N-doped or undoped samples electropolished at 18 V in the given temperature range. The surface results underscored the sensitivity of the N-doped surface to the surface temperature during EP, with the number and dimensions of type-1 pits and possibly microscopic unevenness.

Effect of voltage.—To assess the impact of applied voltage on N-doped surfaces, another set of N-doped samples were electropolished at various voltages ranging from 3 to 22 V while maintaining a surface temperature of approximately 40 °C. An undoped sample was also electropolished at 8 V and 40 °C to compare with the N-doped sample treated under the same EP conditions. The high sample temperature of 40 °C was intentionally chosen to enhance the reaction rate and observe the effect of the applied voltage on surface pitting under the extreme reaction. The EP conditions applied to these samples are detailed in Table II.

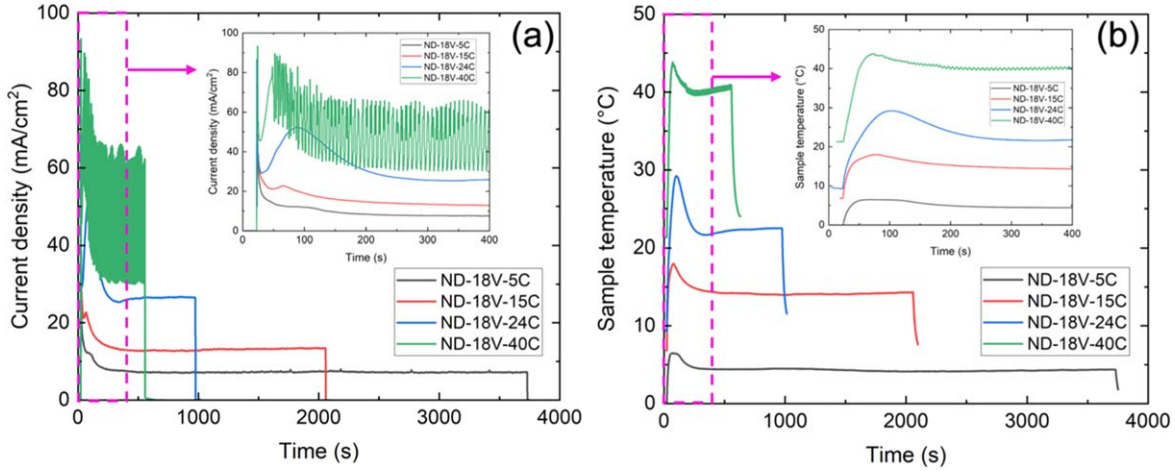

Figure 7. Current densities (a) and sample temperatures (b) during EP of the N-doped samples at a constant voltage of 18 V and various surface temperatures of 5, 15, 24, and 40 °C. Insets: Zoom-in view of the highlighted dotted regions in (a) and (b).

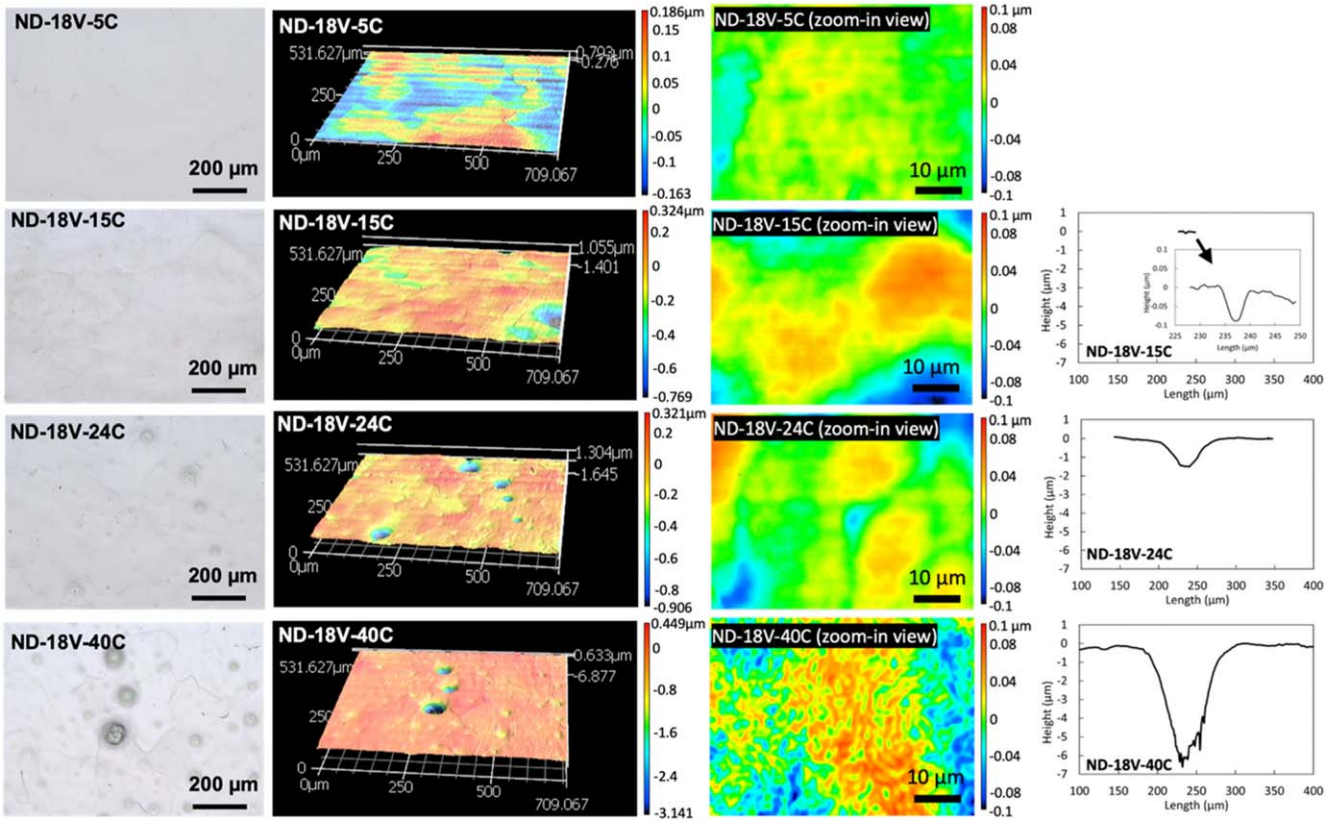

Figure 8. Optical and LCSM images of the N-doped samples ND-18V-5C, ND-18V-15C, ND-18V-24C, and ND-18V-40C after light removal of 5–6 µm in EP. The images with high magnification are labeled as zoom-in view. The right plots show profiles of type-1 pits found on the surfaces.

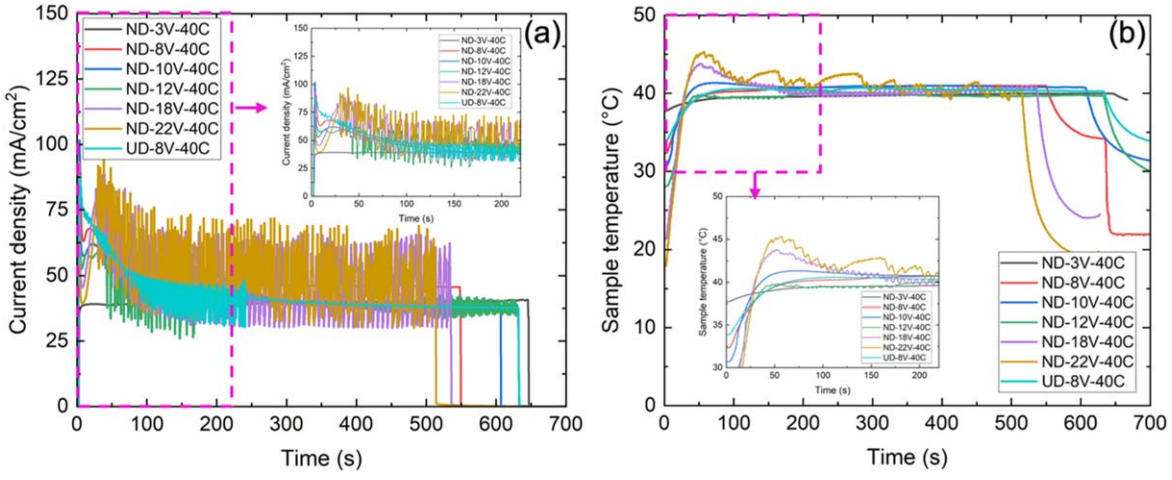

Figure 9. Current density and temperature profiles during EP performed for the N-doped and undoped samples at various voltages ranging from 3 to 22 V and a constant target temperature of 40 °C. Insets: Zoom-in view of the highlighted dotted regions in (a) and (b).

The current density and temperature profiles during EP of these samples are shown in Fig. 9. Except for the first two minutes at the beginning of EP, current densities and temperatures were maintained to be similar for all the samples. Similar to that observed with the samples shown in Fig. 7, the current density profiles for all the N-doped samples showed dips after initial spikes except for ND-3V-40C electropolished at 3 V. Moreover, ND-3V-40C showed no peaks in the current density and sample temperature. Unlike ND-8V-40C, the dip was also not apparent for the undoped sample UD-8V-40C. The dips and post-dip peaks in the current densities and corresponding temperature peaks were pronounced at the higher EP voltages, as seen in the samples ND-18V-40C and ND-22V-40C. Additionally, ND-18V-40C and ND-22V-40C exhibited high amplitude current oscillations, typically observed in EP of Nb material. The repetitive rise and fall in the temperature profile of ND-22V-40C during the EP were due to excess heat generation encountered by the cooling coil to keep the sample temperature close to 40 °C.

Optical and LCSM images of the sample surfaces with different magnifications are presented in Fig. 10. ND-3V-40C, electropolished at a voltage lower than the onset EP voltage, exhibited a rough surface with preferential etching of the grains. As presented in the magnified image of ND-3V-40C, some grains showed protruding features usually observed after low voltage etching of an undoped sample. Pitting on the sample surface was not observed. The sample

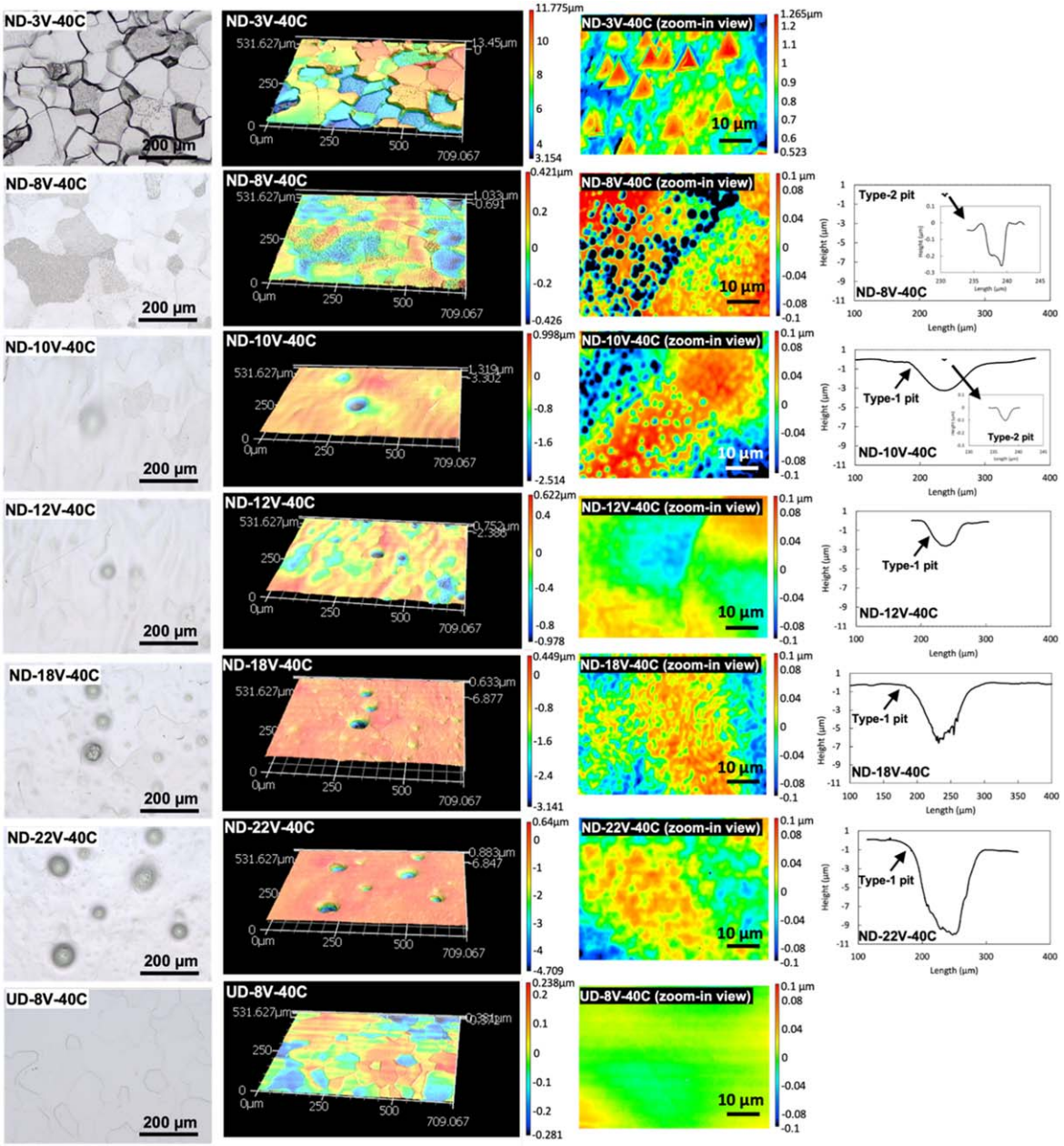

Figure 10. Optical and LCSM images of the N-doped samples ND-3V-40C, ND-8V-40C, ND-10V-40C, ND-12V-40C, ND-18V-40C, ND-22V-40C, and an undoped sample UD-8V-40C after light removal of 5–6 µm in EP. The right plots present type-1 and type-2 pit profiles found on the surfaces. The insets in the plots present type-2 pits on ND-8V-40C and ND-10V-40C surfaces.

ND-8V-40C electropolished at 8 V, which was close to the onset voltage, yielded a macroscopically smooth surface without preferential grain etching. However, the sample surface had sub-micron rough features that appeared different on different grains. The magnified image revealed that these features were dense pits in diameters up to a few microns and a depth of a few hundred nanometers. We considered these pits as type-2 pits based on their small sizes. Also, unlike type-1 pits, these pits were uniformly present on the surface with variations in their sizes from one grain to another. Such features were not found on the undoped sample UD-8V-40C, electropolished at the same voltage and temperature, as shown in Fig. 10. The ND-40C-10V surface was also found to have these type-2 pits but with comparatively lower depths. Growth of large-sized type-1 pits was noticed on the surface of ND-40C-10V and became more significant in terms of pit density and dimension with voltage increase. In contrast to type-1 pits, the type-2 pits became less pronounced with voltage increase. Sample ND-12V-40C also showed signs of type-2 pits, although they were not deep and clear. The type-1 pit density appeared to be higher on ND-12V-40C than that observed on ND-10V-40C. The type-1 pit densities and depths increased on ND-18V-40C and ND-22V-40C, electropolished at 18 and 22 V. These pits on ND-18V-40C and ND-22V-40C were found up to ∼6 and ∼11 µm deep, respectively. As mentioned earlier, microscopic topographic unevenness was observed on ND-18V-40C as well as ND-22V-40C.

The profiles of both types of pits found on the samples are shown along with the images in Fig. 10. The geometry parameters r_e/R and θ for a type-2 pit with $R = 2.1$ µm on ND-8V-40C were estimated to be ∼0.5 and ∼26°, respectively. The parameters were similar to those measured for some deeper type-1 pits with small r_e values. ND-10V-40C and ND-12V-40C showed shallow pits with $r_e/R > 1$ and $\theta < 10°$, respectively. However, pits with non-uniform edges on ND-12V-40C showed lower r_e/R values, such as $r_e/R \sim 1$ and θ of ∼10° for a pit with $R = 13$ µm. Type-1 pits with non-uniform edges

Table II. Electropolishing conditions applied to the undoped and N-doped Nb samples. Pre-process represents the process applied before the final light EP.

		Light EP	
Sample	Pre-process	Sample temperature (°C)	Voltage (V)
UD-8V-40C	Bulk EP	40	8
ND-3V-40C	Bulk EP, 2/0 N-doping	40	3
ND-8V-40C	Bulk EP, 2/0 N-doping	40	8
ND-10V-40C	Bulk EP, 2/0 N-doping	40	10
ND-12V-40C	Bulk EP, 2/0 N-doping	40	12
ND-18V-40C	Bulk EP, 2/0 N-doping	40	18
ND-22V-40C	Bulk EP, 2/0 N-doping	40	22

on ND-22V-40C showed even lower values of r_e/R. As an example, a pit with $R = 43$ μm had $r_e/R \sim 0.15$ and $\theta \sim 16°$.

The results suggest that an EP voltage close to V_o yielded the surface with the type-2 pit formation, which a higher EP voltage could mitigate. However, the higher EP voltages, similar to those observed with the higher surface temperature, lead to the formation of the type-1 pits on the N-doped surface.

Effect of HF concentration.—The concentration of HF in the EP acid directly impacts the EP current density, with higher HF concentrations resulting in higher current densities. Although a systematic study was not conducted to precisely determine the effect of HF concentration on the N-doped surface morphology, acid from the batch-2, which possibly had a higher HF concentration, was used to EP an N-doped sample ND-18V-15C-B at 18 V and 15 °C. This was done to compare the surface with that of ND-18V-15C. Despite both acids being prepared with identical original HF amounts, the evaporation of HF during the mixing of HF and H_2SO_4 may result in different levels of active F^- in the acid. The LCSM image of the ND-18V-15C-B is shown in Fig. 11. A comparison of the surface with that of ND-18V-15C, as shown in Fig. 8, revealed apparent differences in the densities and depths of the type-1 pits. The acid with a higher HF concentration increased the pitting risk on the EP surface.

Physical phenomena during EP.—A physical phenomenon occurring on the N-doped Nb surface during EP was captured using a camera positioned in front of the EP sample, which was placed in a transparent acid bath. The captured image of the sample surface under EP at 18 V and 40 °C is shown in Fig. 12. Before the voltage was applied, no visible bubbles were present on the surface. Once the voltage was turned on, gas bubbles began to form on the surface. Many bubbles were observed sticking to and leaving the surface. The gas evolution was significantly intense during the first two minutes of EP. After approximately 5 μm of material was removed, EP was paused for a minute before being resumed. Bubbles stuck in the viscous layer were quickly removed from the surface when the voltage was turned off. When the voltage was turned on again, no gas evolution was observed except for the presence of a few bubbles on the surface. Bubbles might not reappear on the surface when EP completes even ∼1 μm material removal followed by turning the voltage off and back on. The gas evolution was intense for the N-doped samples treated at higher voltages and temperatures and had larger and deeper type-1 pits on their surfaces. This gas evolution phenomenon confirmed a different chemical reaction on the N-doped surface than on an undoped Nb surface.

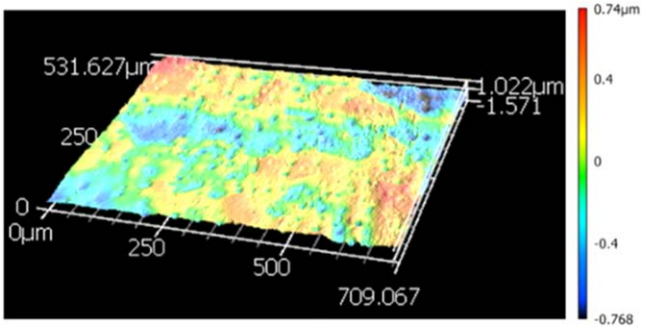

Figure 11. lCSM image of the N-doped surface (ND-18V-15C-B) electropolished at 18 V and 15 °C with the second acid batch potentially having a higher HF concentration.

Another phenomenon was observed during the low-voltage EP and J–V measurement of N-doped samples. After the low voltage EP or a J–V measurement, a dark-gray colored thin layer sliding down the sample surface was visually observed. The film, which broke into tiny flakes, was seen in the EP acid after the J–V measurement or low-voltage EP was completed. These flakes were also found in water used to rinse the N-doped sample after the low-voltage EP. Figure 13 shows the removed layer found in rinsing water. Such peel-off was not seen when the EP voltage was above V_o, as confirmed with other N-doped samples.

Chemical analysis.—To determine the chemical state of the removed top layer, the collected flakes from the rinsing water were analyzed using EDS and XPS. The collected flakes were sprinkled on an adhesive and conductive carbon tape to prepare the sample for the chemical analyses. SEM images with detailed micro-features of the flakes adhered to the tape are shown in Figs. 14a–14c. Various surface features, including pyramid-shaped microstructure, were observed. The pyramid-shaped structures were similar to those observed on the N-doped surface shown in Fig. 4. EDS mapping, as shown in Fig. 14, was performed to attain elemental information. The EDS mapping of the flakes mainly showed Nb with the presence of nitrogen and traces of fluorine. The results indicated that the removed film was the N-rich Nb layer.

To obtain the detailed chemical status of the layer, XPS of the same flakes was performed. Additionally, XPS analysis was conducted for three other samples, including the electropolished reference sample, N-doped sample, and N-doped sample exposed to the EP acid for 4 h. Wide and narrow scans for Nb, O, C, and N were performed. The Nb peaks obtained for these samples are shown in Fig. 15. N 1s spectra for the samples, except for flakes, are shown in Fig. 15e. The intensity of the N 1s spectrum for the removed layer was very low because the adhesive tape was not well covered with the flakes. The Nb peak for the flakes was also less intense compared to the bulk samples. The undoped reference surface showed two intense peaks of Nb $3d_{5/2}$ at 207.7 and 202.5 eV, representing Nb^{5+} and Nb^0 states of Nb. The other three samples showed an additional peak of Nb $3d_{5/2}$ at 203.5 eV, representing the nitride phase of Nb.[28] Two intense N peaks in the N 1s spectra of both N-doped and acid-exposed N-doped surfaces included two peaks at 396.8 and 398 eV, which represented NbN and niobium oxy-nitride (NbN_xO_y),

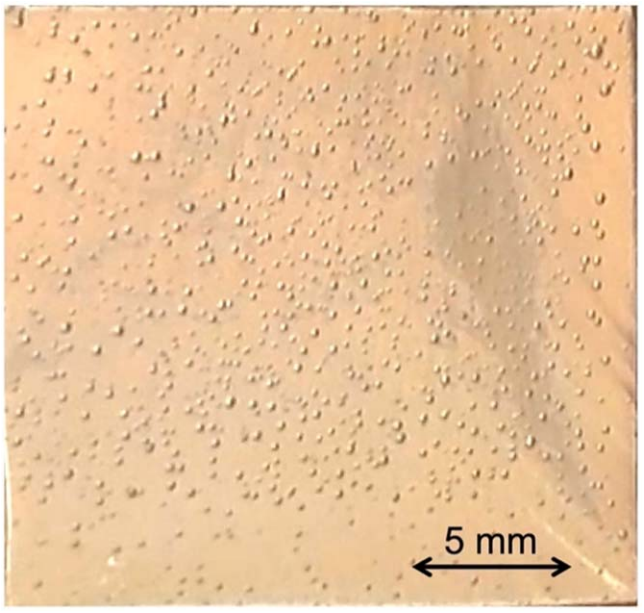

Figure 12. Gas evolution forming bubbles on an N-doped Nb sample surface (20 × 20 mm) during EP at 18 V and sample temperature of 40 °C.

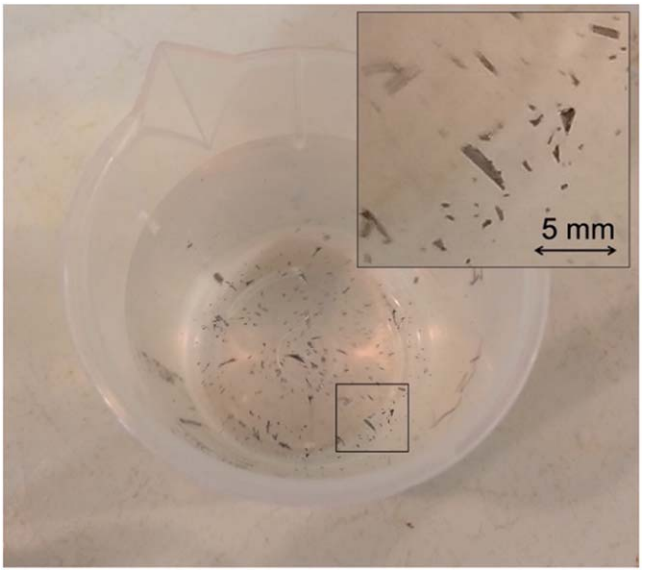

Figure 13. Water used to rinse the N-doped Nb sample after EP at 3 V in the etching regime. Inset: the magnified view of the flakes available in the highlighted box.

respectively. The Nb^{5+} and nitride peaks in the Nb spectrum of the peeled-off layer indicated that the layer contained Nb in nitride and oxide forms. The Nb 3 d and N 1s spectra, which are identical to the spectra of the N-doped surface and show nitride peaks for the acid-exposed N-doped surface, revealed that the nitride layer present on the surface was not dissolved during the EP acid exposure.

Two-step EP process.—Since low voltage or *J–V* measurement removed the top layer from the N-doped surface, a *J–V* measurement was added at the beginning of EP to remove the nitride layer and evaluate its effect on the N-doped surface. As shown in Table III, four N-doped samples were electropolished with the standard and two-step EP processes for light removal of ∼7 μm. In the two-step EP process, initially, the samples ND-18V-40C-P and ND-18V-12C-P underwent a *J–V* measurement from 0 to 20 V, with voltage increments of 1 V every 12 s. Subsequently, the samples ND-18V-40C-P and ND-18V-12C-P were electropolished at 40 and 12 °C, respectively, and at 18 V. The higher temperature and stronger electrolyte from batch-2 were used for EP to maximize the reaction rate, which could increase surface pitting severity. To compare the surfaces with the standard EP surfaces, ND-18V-40C-B and ND-18V-12C-B were electropolished at 40 and 12 °C in the same acid bath and at the same voltage of 18 V.

J–V curves and current density and temperature curves as a function of elapsed time during two-step EP are shown in Fig. 16. The *J–V* curves measured at different temperature ranges of 4 °C–12 °C and 20 °C–40 °C represent similar V_o of 6–7 V. The removal thicknesses in the etching regime between 0 to 6 V for ND-18V-40C-P and ND-18V-12C-P were ∼0.25 and 0.12 μm, respectively, estimated using the total charge and Faraday's law.

Optical and LCSM images of the sample surfaces after the standard and two-step EP processes are shown in Fig. 17. The ND-18V-40C-B surface showed dense and deep type-1 pits, which were even more profound than those observed on ND-18V-40C electropolished using the electrolyte from the batch-1. The ND-18V-12C-B surface, electropolished at 12 °C, also had type-1 pits. However, these pits were shallow and less dense compared to ND-18V-40C-B. The effect of temperature on type-1 pits is consistent with that observed with other samples shown in Fig. 8. In contrast, the ND-18V-40C-P and ND-18V-12C-P surfaces, which underwent the two-step EP process, showed no noticeable type-1 pits. This indicates that the two-step EP process effectively mitigates the large-sized type-1 pits on the surface, even at elevated EP temperatures. No significant preferential grain etching due to the initial low voltage application was observed when the surface received 5–7 μm EP in the current plateau regime.

The magnified images of the samples in Fig. 17 show the microscopic features of the uneven spots found on their surfaces. All samples were found to have some grains with uneven surfaces. The grains with rough surfaces in the ND-18V-40C-B and ND-18V-40C-P showed unevenness with ∼100 nm height variation. The surfaces of ND-18V-12C-B and ND-18V-12C-P also displayed microscopic unevenness, but the uneven spots were less widely distributed and smoother compared to their 40 °C counterparts. For these low-temperature electropolished samples, the surface height variation was within a few tens of nanometers. This observation suggested that the two-step EP process could not minimize the unevenness of the N-doped Nb surface. However, low-temperature EP appeared to control over topographic unevenness.

The surfaces were examined with SEM to inspect for tiny pits in size within a few microns that may not be clearly resolved using LCSM. The SEM images of the samples are shown in Fig. 18. Other than the uneven surfaces, no tiny pin holes or pits were visible in the SEM images.

Discussion

XPS analysis of the N-doped surface confirmed the presence of nitride phases, as reported earlier.[10,14,15,28] The Nb peak at 203.5 eV, reflecting nitrided niobium, and the N 1s spectrum with peaks at 396.8 and 398 eV, assigned to niobium nitride and oxy-nitride phases respectively, corroborated these findings.[28,29] Although not shown in this paper, the C peak was used to check for any carbide precipitates on the N-doped surface. No sign of carbide, which usually appears at a binding energy of ∼282.8 eV,[30,31] was observed within the detection limit of XPS.

The N-doped surfaces, due to the presence of a niobium nitride layer, exhibited distinct electrochemical behavior compared to undoped surfaces when subjected to EP under standard electrolyte and EP conditions. This different behavior was evident from the pitting on the surface and gas evolution phenomenon. Moreover, the current density dips, which might represent the formation of a passive oxide layer on the surface, differed for the samples ND-8V-40C and UD-8V-40C. The different dips might indicate that the

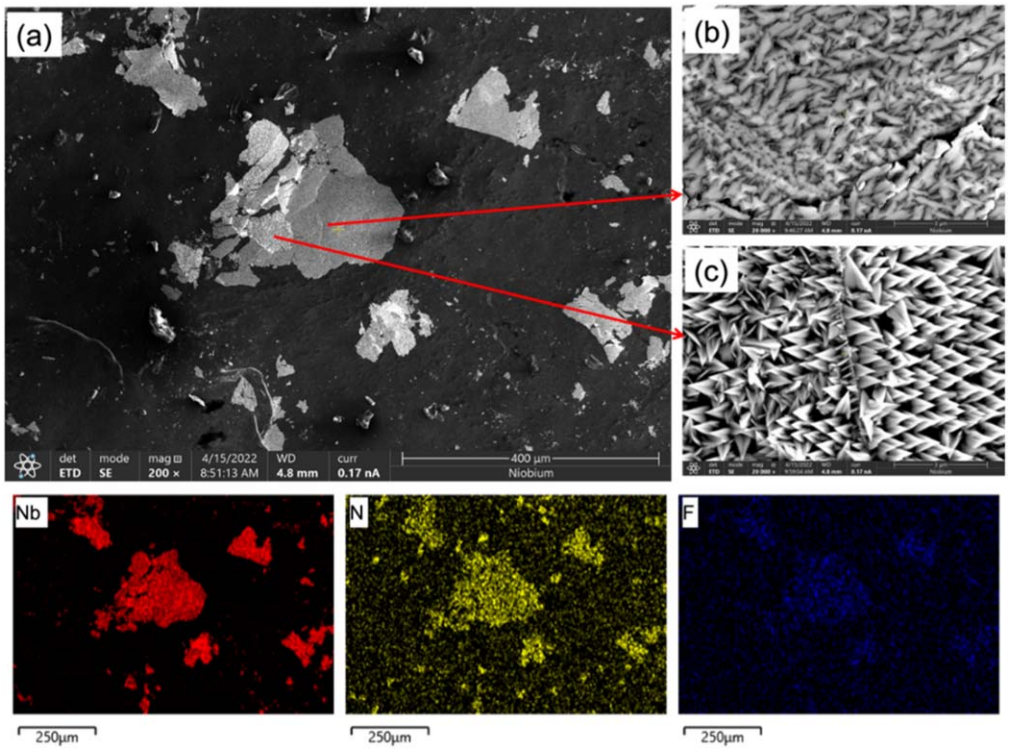

Figure 14. (a) Top layer removed from the N-doped surface in electrochemical etching performed in the etching regime of the *J–V* curve. (b) and (c) Two different grains having different microstructures. The bottom three images show EDS maps of Nb, N, and F for the region shown in (a).

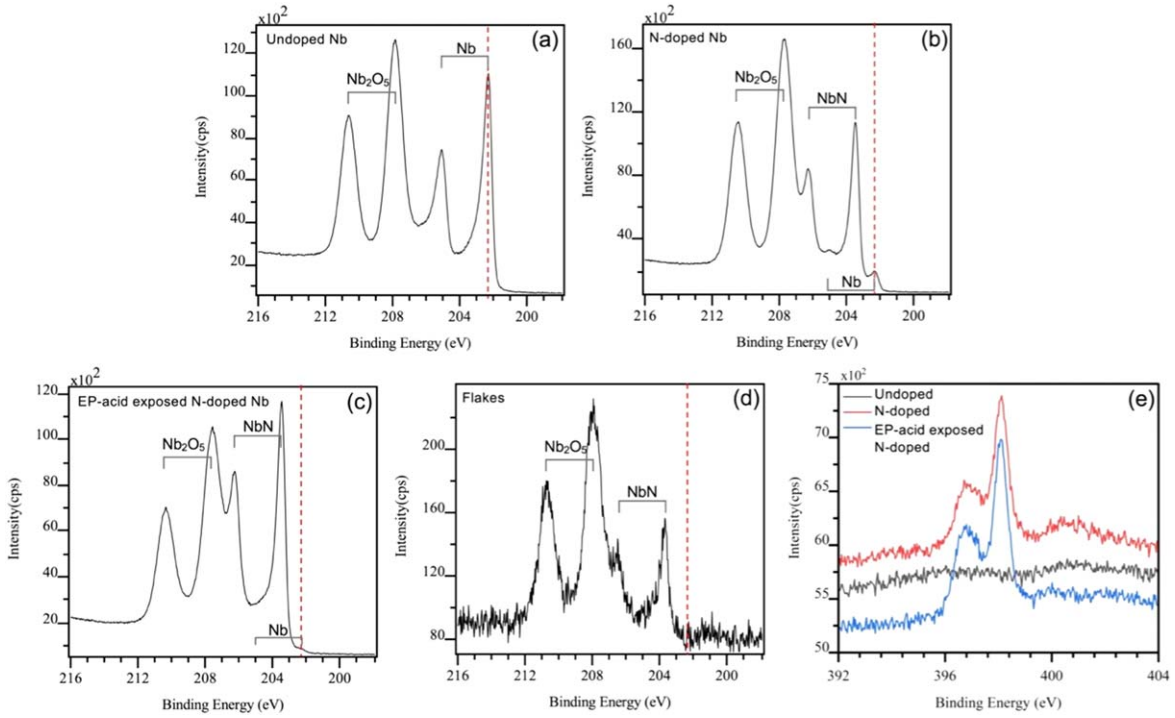

Figure 15. Nb 3d spectra of the top surface of (a) electropolished Nb sample (b) N-doped Nb sample (c) N-doped sample immersed in the EP acid for 4 h, and (d) flakes removed from N-doped surface in EP. The dotted vertical lines represent the binding energy for Nb^0. (e) N 1s spectra of the electropolished undoped, N-doped, and acid-exposed N-doped surfaces.

surfaces have slightly different passive layer thicknesses at the same voltage. This effect was not seen at higher voltages because a higher voltage can form a thicker passive layer on N-doped and undoped surfaces. The thicker oxide formation can be observed as more pronounced dips in higher voltage cases. A higher polarization resistance due to a thicker passive layer on the Nb surface at a higher EP voltage has been reported.[25] Dissolution of the thicker oxide produced a higher current peak after the dip. *J–V* curves usually express such differences in the onset. However, the similar onset in the *J–V* curves measured for undoped and N-doped could be because

Table III. Conditions for the standard and two-step EP applied to N-doped Nb samples using EP acid with an increased HF concentration. Pre-process represents the process applied before the final light EP.

		Light EP		
Sample	Pre-process	EP type	Sample temperature (°C)	Voltage (V)
ND-18V-40C-B	Bulk EP, 2/0 N-doping	Standard	40	18
ND-18V-40C-P	Bulk EP, 2/0 N-doping	Two-step	40	18
ND-18V-12C-B	Bulk EP, 2/0 N-doping	Standard	12	18
ND-18V-12C-P	Bulk EP, 2/0 N-doping	Two-step	12	18

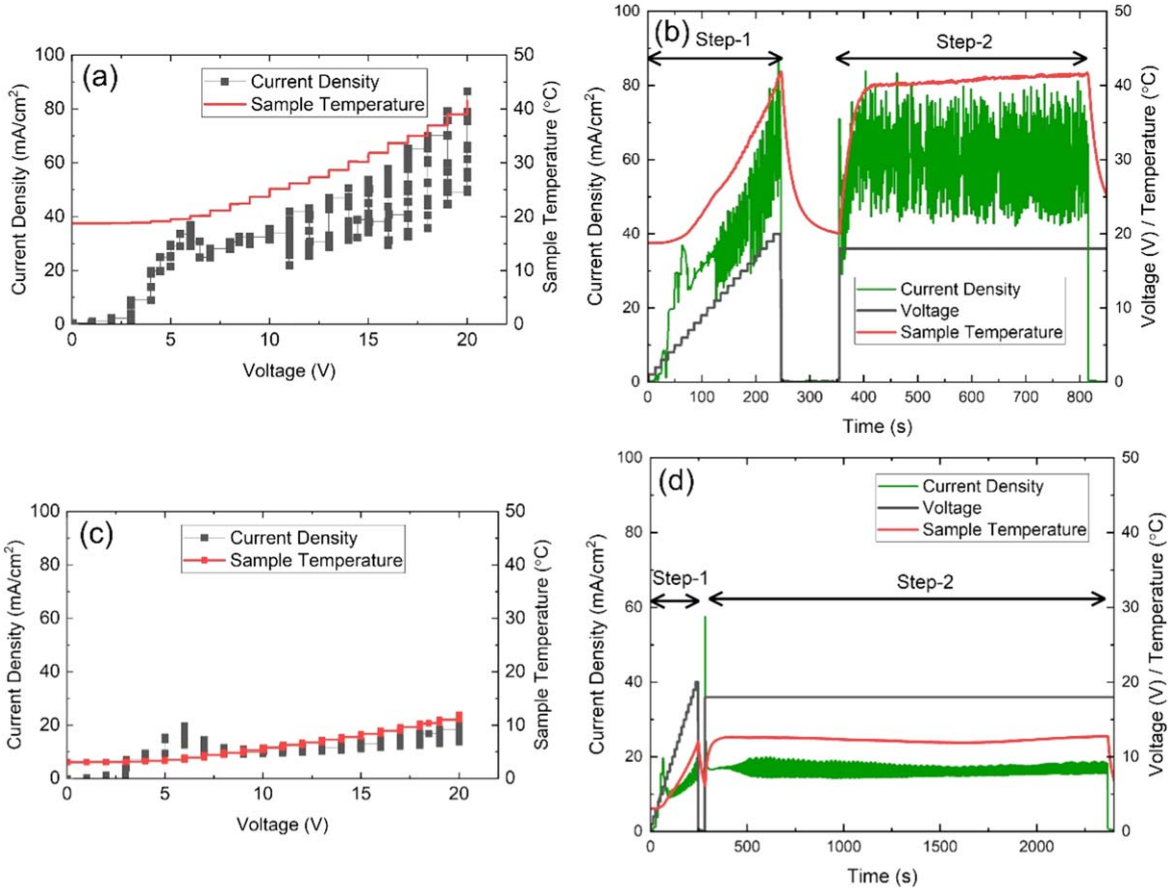

Figure 16. *J–V* curve recorded during the first step of the two-step EP process for samples (a) ND-18V-40C-P and (c) ND-18V-12C-P. (b) Current density, surface temperature, and voltage profiles during the two-step EP process applied to the samples (c) ND-18V-40C-P and (d) ND-18V-12C-P.

the 200–300 nm thick top nitride layer, where the thickness corroborated with the previous finding,[10,28] left the surface in the etching regime of the *J–V* measurement.

The peeling of the nitride layer might be caused by the etching of the underneath Nb material holding the nitride layer. It is to be noted that the acid exposure without applied voltage and EP in the diffusion-limited conditions were incapable of peeling off the layer. A voltage above the onset that forms a passive oxide film on the EP surface might avoid the etching of the underneath Nb material.

Pitting initiation is usually attributed to local damage of a surface's passive layer in extreme environments, like the presence of Cl^- ions, exposing the electrode to accelerated material dissolution and leading to pit formation. Like chloride, fluoride ions have also been found to initiate pitting corrosion, as reported for titanium and titanium alloy in solutions containing fluoride.[32,33] Pit initiation becomes significantly high for electrodes with inhomogeneities caused by factors such as the inclusion of impurities, alloying, precipitation, and surface roughness.[34] Reference 34 also highlighted that the growth of pits might be caused by electrochemical heterogeneity, representing distinct reactions over the electrode surface. The N-doped surface has inhomogeneities due to nitrogen inclusion and nitride precipitation. Moreover, the multiphase surface, due to niobium oxide and nitride, satisfies electrochemical heterogeneity. These conditions might make the N-doped surface susceptible to pitting initiation and growth in an electrolyte containing F. Type-2 pits, as observed on the ND-8V-40C and ND-10V-40C, were attributed to inhomogeneous EP at low voltages, discussed later in this section. These pits uniformly appeared on the surface with variation between grains, likely influenced by differences in grain orientation. Although most of these pits appeared bigger than those reported in Refs. 23, 24, small pits were comparable.

As stated earlier, the N-doped samples with type-1 pits on their surfaces also showed gas evolution and bubble formation. Type-1 pit formation could be initiated by gas bubbles formed on the surface due to gas evolution. Gas evolution and pit formation can be explained as

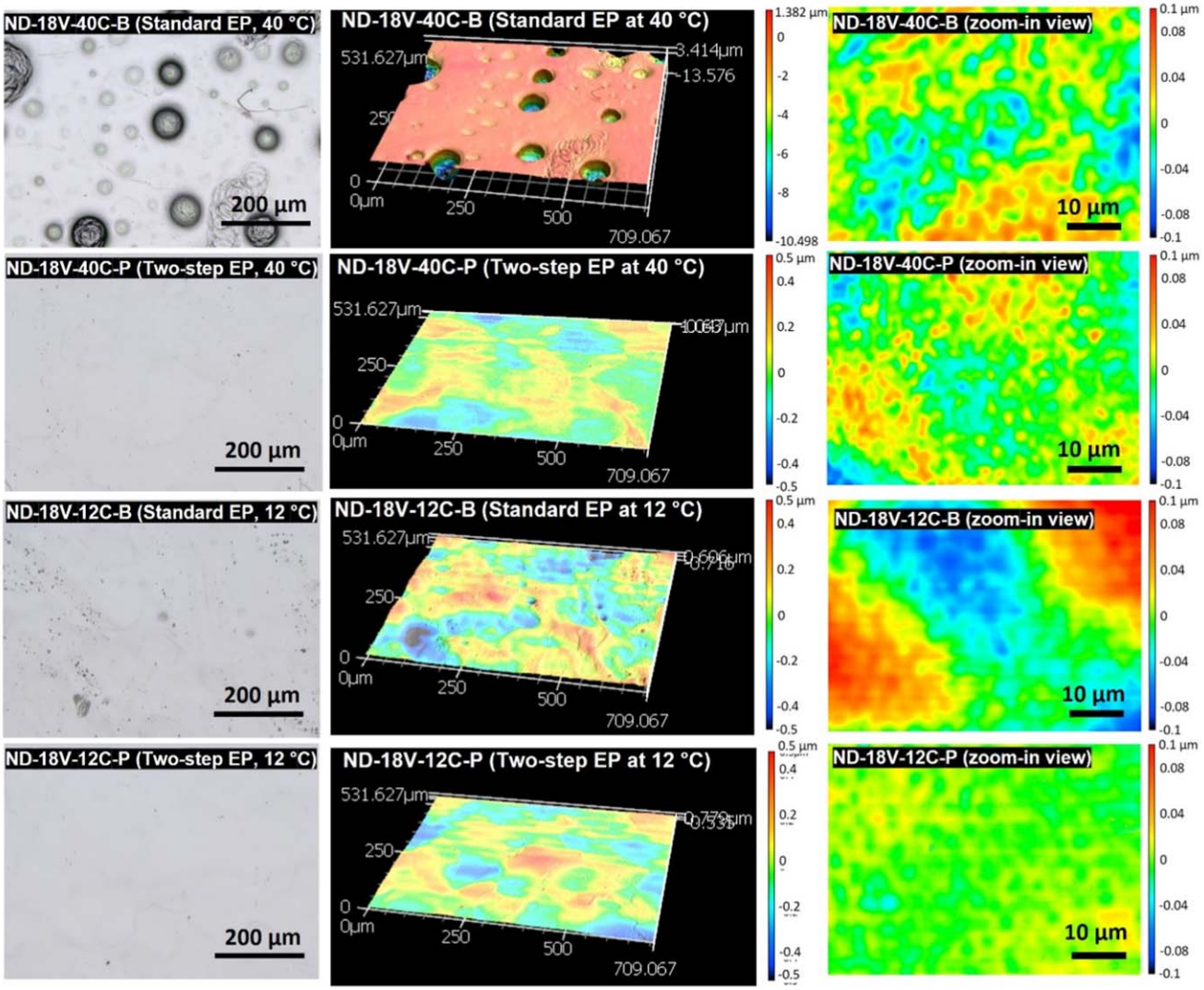

Figure 17. lCSM images of N-doped samples subjected to standard and two-step EP at 40 °C and 12 °C. The images (57 × 43 μm^2) in the right show zoom-in view of the grain surfaces found with unevenness.

follows. The gas evolution phenomenon often occurs in electrochemical reactions and depends on the type of electrolyte, electrode material, and applied electrochemical conditions. The NbN layer on the N-doped surface, compared to the undoped Nb surface, was found to be responsible for evolving gas, possibly oxygen. Oxygen evolution might be the result of water electrolysis occurring on the niobium nitride electrode.[35] Transition metal nitrides, including NbN, have superior electrocatalytic performance for water electrolysis compared to base metals.[36–38] Gas bubbles adhered to the viscous acid layer on the surface and detached from it. The bubbles shielding the EP surface reduce the local reaction rate.[39] On the other hand, the detachment and collapsing of bubbles might impair the viscous layer locally, leading to an aggressive reaction. Pit formation on EP surfaces has been attributed to the broken bubble tunneling effect.[40] The effects of bubbles on the surface morphology of Nb and higher material removal in the EP process have been reported elsewhere.[11] The type-1 pits on the surface were formed mainly in the first few minutes of EP when many bubbles left the surface. This was confirmed in an EP experiment performed to remove ~1.8 µm thick layer at 40 °C and 18 V, followed by a voltage-off period for 1–2 min to release the bubbles from the viscous layer and resume EP to complete 6 µm EP at the same temperature and voltage. The sample surface showed pits similar to those found on the ND-18V-40C sample.

The applied EP voltage ranges, which correspond to different regimes in the *J–V* curve, significantly affect pitting on the N-doped surface. The pit formation was not noticeable at a low voltage of 3 V, which lies in the etching regime in the *J–V* curve. No surface pitting at the low voltage might be due to the peeling-off of the nitride layer in the etching regime. However, below the onset voltage, preferential grain etching occurred,[21] yielding a rough surface. The type-2 pits were found in the medium voltage range, from V_o to a few voltages above V_o. The formation of type-2 pits near the onset is consistent with the previous finding.[41] In this medium voltage range, the passive oxide layer might not be thick and uniform enough to suppress inhomogeneous EP on the oxide and nitride surfaces. This hypothesis is supported by the ND-18V-40C and ND-22V-40C surfaces, which possibly had a thicker passive layer due to higher EP voltage and did not have apparent type-2 pits.

It is possible that nitride etching might occur at the beginning of low-voltage etching before the nitride layer detaches from the surface. Shallow type-2 pits might also form on the surface at the beginning of high-voltage EP, especially at higher temperatures that could make the passive layer thinner. When EP completes 5–7 µm removal, these pits disappear or become shallower, making the surfaces uneven in tens of nanometer scale. References 23, 24 represented that pits were present on the N-doped surfaces with a greater depth after 1 µm removal, and the pits became less significant with removal in EP.

Additionally, our study shows that a higher reaction rate alone does not cause type-1 pitting unless the applied voltage exceeds a

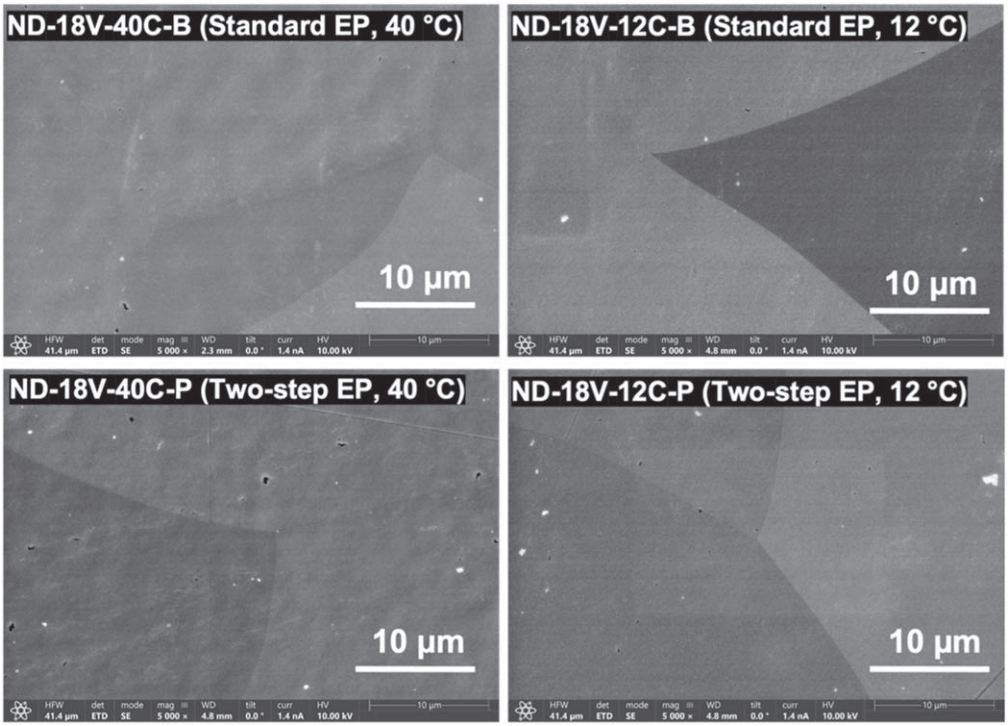

Figure 18. SEM images of N-doped samples treated with (top) standard EP and (bottom) two-step EP at 40 and 12 °C. EP was conducted in the batch-2 acid bath with an increased HF concentration.

certain threshold. EP tests at 40 °C with similar current densities at various voltages revealed that the type-1 pit formation started when the applied voltage was around 10 V, which might be sufficient for water electrolysis on the nitride surface. Further higher voltage significantly enhanced the gas evolution as the gas evolution rate might exponentially increase with applied voltage.[42] As a result of more and larger bubbles on the surface at a high voltage, the number of pits and their dimensions increased significantly.

The enhanced reaction rate, either due to a higher surface temperature or a higher HF concentration in the acid, promotes gas evolution and the type-1 pit formation on N-doped surfaces. Gas evolution was observed even at low temperatures (e.g., 12 °C), but bubbles were smaller due to slower reaction rates and water electrolysis. The effect of temperature on type-2 pit formation at an EP voltage close to V_o was insignificant. Type-2 pits with depths similar to those observed on ND-8V-40C also formed on an N-doped surface at a lower temperature of 22 °C during EP performed at 7 V, though this result is not included in the result section. The passive layer at 7–8 V, even at a low temperature, might remain thin. A low temperature in the etching regime might reduce nitride etching by reducing average removal before the nitride layer peels off. High voltage, along with a low temperature, might form a thicker passive film and prevent deeper type-2 formation and nitride etching. This could explain why low temperatures minimized the microscopic topographic unevenness.

Since the deeper pits on the N-doped surface were found with lower r_e/R and higher θ, both types of deep pits may contribute to enhancing β_M values to approximately 1.2–1.3. The value was estimated using the β_M vs r_e/R curves provided in Ref. 5. Further study is required to evaluate β_M for various pit geometries, including the shallow pits and bubble traces identified in this study. Acid agitation in the cavity EP could reduce type-1 pit density and depth. For the 1.3 GHz cavity, electropolishing at 15 °C and a voltage several volts higher than the onset might produce type-1 pits shallower than those found on ND-18V-15C. These shallow pits might not affect the cavity performance. For large-sized cavities, such as 650 MHz cavities, EP requires a higher voltage of 20–25 V.[26] This higher voltage could prevent type-2 pitting but can enhance gas evolution, increasing the risk of type-1 pit formation. The irises of these larger elliptical cavities might be even at higher risk for gas evolution and pitting due to their lower EP onset voltage resulting from proximity to the cathode. When bubbles are formed on the cavity surface, they can lead to bubble traces and pits on the surface. Pitting on the equator might contribute to the magnetic field enhancement locally to some extent to reduce the quench field.

For such large-sized cavities, the two-step EP method may be crucial to reduce type-1 pits on the surface. The two-step EP appeared promising to mitigate type-1 pits even at standard applied voltage and surface temperature used for cavity EP. However, as stated earlier, high-temperature EP at 40 °C with a high HF concentration in the EP acid could form an uneven microscopic surface. The removal during the *J*–*V* measurement must be kept to a minimum to only peel off the nitride layer. This could minimize the surface unevenness and preferential grain etching. The ND-18V-12C-P surface, which experienced *J*–*V* measurement to remove only 0.12 µm in the etching regime, was found to have no noticeable type-1 pit and a smoother microscopic surface. The microscopic surface smoothness could also be improved with acid agitation. Nitride layer peeling in the first step can also be achieved by applying a constant low voltage. Further study would be needed to determine whether further lower removal in the etching regime can peel the layer off. This could be achieved with a relatively higher voltage scanning rate, lower temperature, and lower HF concentration.

Conclusions

We studied the effect of EP parameters on N-doped and undoped Nb surfaces. The standard EP conditions, optimized for undoped Nb, were found to be inadequate for N-doped surfaces since the thin nitride layer on the N-doped Nb surface made it susceptible to pitting. The pits observed on the surfaces were defined as type-1 and type-2 based on their characteristics and diameters. The type-1 pits, typically larger than 5 µm, formed in the high voltage range of the EP plateau and might be caused by gas evolution on the surface. These pits were randomly found on the surface. The type-2 pits, smaller in diameter than 5 µm, were formed in EP at the medium voltage range, from the onset to a few volts above it. The formation

of type-1 pits was reduced by lowering the reaction rate, either through decreased surface temperature or reduced HF concentration in the electrolyte. Type-2 pits could be mitigated by selecting an appropriate voltage well above the onset. However, a high EP voltage, while mitigating type-2 pits, enhances the risk of type-1 pitting, thus highlighting the trade-offs involved in the EP process.

To address voltage sensitivity and avoid pitting, a two-step EP process was developed. In this process, the nitride layer is initially removed in the etching regime before applying the standard EP conditions to achieve the desired material removal. The two-step EP process mitigated the type-1 pits, even under an extreme reaction rate and high voltages. However, the surface at higher temperatures can become uneven on a scale of 100 nm. To keep the topographic unevenness low, low-temperature EP should be considered. The sample ND-18V-12C-P subjected to two-step EP at a lower temperature of 12 °C was found with no observable type-1 pits and with a smoother microscopic surface.

Acknowledgments

This manuscript has been authored by Fermi Forward Discovery Group, LLC under Contract No. 89243024CSC000002 with the U.S. Department of Energy, Office of Science, Office of High Energy Physics. The authors thank Prof. Shigeki Kato, KEK, for providing the facility for XPS analysis.

ORCID

V. Chouhan https://orcid.org/0000-0002-8200-4931

References

1. K. Saito, H. Inoue, E. Kako, T. Fujino, S. Noguchi, M. Ono, and T. Shishido, "Superiority of electropolishing over chemical polishing on high gradients." *Proceedings of the 8th Workshop on RF Superconductivity (SRF1997), Abano Terme Padova, Italy*, (Padova, Italy), (INFN), 795 (1998), (1997).
2. J. Knobloch, R. L. Geng, M. Liepe, and H. Padamsee, "High-field Q slope in superconducting cavities due to magnetic field enhancement at grain boundaries." *Proceedings of the 1999 Workshop on RF Superconductivity, Santa Fe, NM* (CERN), (Geneva), 77 (1999).
3. D. Meidlinger, "Basic understanding for the various causes of quench." *Proceedings of the 14th International Conference on RF Superconductivity (SRF2009)* (Berlin, Germany), 117 (2009).
4. Y. Xie and M. Liepe, "New insights into quench caused by surface pits in SRF cavities." *Proceedings of the International Conference on RF Superconductivity (SRF2013), Paris, France*, (JaCoW, Geneva, Switzerland), 378 (2013).
5. T. Kubo, "Magnetic field enhancement at a pit on the surface of superconducting accelerating cavity." *Prog. Theor. Exp. Phys.*, 073G01**16** (2015).
6. M. S. Champion, L. D. Cooley, C. M. Ginsburg, D. A. Sergatskov, R. L. Geng, H. Hayano, Y. Iwashita, and Y. Tajima, "Quench-limited SRF cavities: failure at the heat-affected zone." *IEEE Trans. Appl. Supercond.*, **19**, 1384 (2009).
7. Y. Yamamoto, H. Hayano, E. Kako, S. Noguchi, T. Shishido, and K. Watanabe, "Achieving high gradient performance of 9-cell cavities at KEK for the international linear collider." **729**, 589 (2013), 10.1016/j.nima.2013.08.050.
8. Y. Xie and H. Padamsee, "Relationship between defects and pre-heating and defects size." *Proceedings of the 14th International Conference on RF Superconductivity* (SRF, Berlin, Germany) 334 (2009).
9. A. Grassellino et al., *Supercond. Sci. Technol.*, **26**, 102001 (2013).
10. A. Grassellino, A. Romanenko, S. Posen, Y. Trenikhina, O. Melnychuk, D. A. Sergatskov, M. Merio, M. Checchin, and M. Martinello, "N doping: progress in development and understanding." *Proceedings of the 17th International Conference on RF Superconductivity (SRF2015), Whistler, Canada*, (JACoW, Geneva, Switzerland) 795 (2015).
11. D. Bafia, A. Grassellino, A. Romanenko, O. S. Melnychuk, D. A. Sergatskov, D. Bice, A. D. Palczewski, D. Gonnella, and J. F. Zasadzinski, "New insights in the quench mechanism in nitrogen doped cavities." *Proceedings of the 19th International Conference on RF Superconductivity (SRF2019), Dresden, Germany*, (JACoW, Geneva, Switzerland), 3528 (2019).
12. D. Gonnella et al., *J. Appl. Phys.*, **117**, 023908 (2015).
13. M. Martinello et al., "Q-factor optimization for high-beta 650 MHz cavities for PIP-II." *J. Appl. Phys.*, **130**, 174501 (2021).
14. Y. Trenikhina, A. Grassellino, O. Melnychuk, and A. Romanenko, "Characterization of nitrogen doping recipes for the Nb SRF cavities." *Proceedings of the 17th International Conference on RF Superconductivity (SRF2015), Whistler, Canada* (JACoW, Geneva, Switzerland) 223 (2015).
15. P. Dhakal, "Nitrogen doping and infusion in SRF cavities: a review." *Physics Open*, **5**, 100034 (2009).
16. B. Gajar, S. Yadav, D. Sawle, K. K. Maurya, A. Gupta, R. P. Aloysius, and S. Sahoo, *Substrate Mediated Nitridation of Niobium into Superconducting Nb2N thin films for phase slip study* (2019), 88119.
17. K. Saito, "Techniques of SC cavity performance for high gradient." *Proceedings of the XXI Linear Accelerator Conference (LINAC2002), Gyeongju, Korea* (Pohang Accelerator Laboratory, Pohang, Korea), 534 (2002).
18. C. E. Reece, A. C. Crawford, and R. L. Geng, "Improved performance of JLAB 7-cell cavities by electropolishing." *Proceedings of the 23rd Particle Accelerator Conference, Vancouver, Canada* (Piscataway, NJ)(IEEE, Piscataway, NJ), 2126 (2009).
19. A. C. Crawford, "Extreme diffusion limited electropolishing of niobium radiofrequency cavities." *Nucl. Instrum. Methods Phys. Res., Sect. A*, **849**, 5 (2017).
20. V. Chouhan, S. Kato, K. Nii, T. Yamaguchi, M. Sawabe, H. Hayano, and Y. Ida, "Effort towards symmetric removal and surface smoothening of 1.3 GHz niobium single-cell cavity in vertical electropolishing using a unique cathode." *Phys. Rev. Accl. Beams*, **20**, 083502 (2017).
21. V. Chouhan et al., "Vertical electropolishing for 1.3 GHz single- and nine-cell superconducting niobium cavities: a parametric optimization and rf performance." *Phys. Rev. Accl. Beams*, **22**, 103101 (2019).
22. M. Checchin, *LCLS-II-HE, Americas Workshop on Linear Colliders* (2020).
23. E. M. Lechner, J. W. Angle, C. Baxley, M. J. Kelley, and C. E. Reece, "Topographic evolution of heat-treated Nb upon electropolishing for superconducting rf applications." **26**, 103101 (2023).
24. J. K. Spradlin, A. D. Palszewski, H. Tian, and C. E. Reece, "Analysis of surface nitrides created during "doping" heat treatments of niobium." *Proceedings of the 19th International Conference on RF Superconductivity (SRF2019), Dresden, Germany*, (JACoW, Geneva, Switzerland)106 (2019).
25. H. Tian, S. G. Corcoran, C. E. Reece, and M. J. Kelley, "The mechanism of electropolishing of niobium in hydrofluoric–sulfuric acid electrolyte." *J. Electrochem. Soc.*, **155**, D563 (2008).
26. V. Chouhan et al., "Electropolishing parameters study for surface smoothening of low- 650 MHz five-cell niobium superconducting radio frequency cavity." *Nucl. Instru. Meth Phys. A*, **1051**, 168234 (2023).
27. H. Tian and C. Reece, "Evacuation of the diffusion coefficient of fluorine during the electropolishing of niobium,." *Phys. Rev. ST Accl. Beams*, **13**, 083502 (2010).
28. A. D. Pandey, G. D. L. Semione, A. Prudnikava, T. F. Keller, H. Noei, V. Vonk, Y. Tamashevich, E. Elsen, B. Foster, and A. Stierle, *J. Mat. Sci.*, **53**, 10411 (2018).
29. A. Prudnikava, Y. Tamashevich, S. Babenkov, A. Makarova, D. Smirnov, V. Aristov, O. Molodtsova, O. Kugeler, J. Viefhaus, and B. Foster, "Systematic study of niobium thermal treatments for superconducting radio frequency cavities employing X-ray photoelectron spectroscopy." *Supercond. Sci. Technol.*, **35**, 065019 (2022).
30. J. C. Ding, W. Dai, T. F. Zhang, P. Zhao, J. M. Yn, K. H. Kim, and Q. M. Wang, "Microstructure and properties of Nb-doped diamond-like carbon films deposited by high power impulse magnetron sputtering." *Thin Solid Film*, **663**, 159 (2018).
31. S. Schelz, P. Reinke, and P. Oelhafen, "A monolayer interface of plasma-polymerized polystyrene on niobium: an in situ electron spectroscopy study." *Surf. Sci.*, **293**, 275 (1993).
32. X. Li, L. Wang, L. Fan, M. Zhong, L. Cheng, and Z. Cui, "Understanding the effect of fluoride on corrosion behavior of pure titanium in different acids." *Corros. Sci.*, **192**, 109812 (2021).
33. J. Li, C. Zhu, F. Cao, and Q. Sun, "Nanoscale pitting corrosion of commercially pure Ti in solution containing fluoride ion." *Mater. Chem. Phys.*, **323**, 129650 (2024).
34. Y. Tan, "Understanding the effects of electrode inhomogeneity on pitting corrosion initiation on bare electrode surfaces." *Corros. Sci.*, **53**, 1845 (2011).
35. M. Azuma, Y. Nakato, and H. Tsubomura, "Stable and efficient electrochemical evolution of oxygen and chlorine on niobium nitride amorphous thin films prepared by the reactive RF sputtering technique." *Mater. Res. Bull.*, **22**, 527 (1987).
36. L. Lin, S. Piao, Y. Choi, L. Lyu, H. Hong, D. Kim, J. Lee, W. Zhang, and Y. Piao, "Nanostructured transition metal nitrides as emerging electrocatalysts for water electrolysis: Status and changes." *EnergyChem*, **4**, 100072 (2022).
37. R. Jamil, R. Ali, S. Loomba, J. Xian, M. Yousaf, K. Khan, B. Shabbir, C. F. McConville, A. Mahmood, and N. Mahmood, "The role of nitrogen in transition-metal nitrides in electrochemical water splitting." *Chem Catalysis*, **1**, 802 (2021).
38. X. Yan, D. Deng, S. Wu, H. Li, and L. Xu, "Development of transition metal nitrides as oxygen and hydrogen electrocatalysts." *Chinese Journal of Structural Chemistry*, **41**, 2207004 (2022).
39. X. Deng, F. Yang, Y. Li, J. Dang, and M. Ouyang, "Quantitative study on gas evolution effects under large current density in zero-gap alkaline water electrolyzers." *J. Power Sources*, **555**, 232378 (2023).
40. S. J. Lee, Y. H. Chen, and J. C. Hung, "The investigation of surface morphology forming mechanisms in electropolishing process." *Int. J. Electrochem. Sci.*, **7**, 12495 (2012).
41. E. Viklund, D. Seidman, T. Ring, and L. Grasselino, "Studies on the fundamental mechanisms of niobium electropolishing." *Proceedings of the 20th International Conference on RF Superconductivity (SRF2021), Michigan, USA*, (JACoW, Geneva, Switzerland), 50 (2021).
42. R. R. Rao, I. E. L. Stephens, and J. R. Durrant, "Understanding what controls the rate of electrochemical oxygen evolution." *Joule*, **5**, 16 (2021).